Acta Mech 229, 1183–1196 (2018)
https://doi.org/10.1007/s00707-017-2032-z

ORIGINAL PAPER

Mohammad Reza Barati

Vibration analysis of porous FG nanoshells with even and uneven porosity distributions using nonlocal strain gradient elasticity

Received: 16 July 2017 / Revised: 2 September 2017 / Published online: 10 November 2017

Abstract This paper studies the free vibrational behavior of porous functionally graded nanoshells using nonlocal strain gradient theory. A nonlocal parameter and a strain gradient parameter are employed to describe both stiffness reduction and stiffness enhancement of nanoshells. Porosities are evenly and unevenly distributed thorough the thickness of the nanoshell. The gradation of material properties having porosities is described using a modified power-law function. The nanoshell is modeled via first-order shear deformation theory, and Galerkin's method is implemented to obtain vibration frequencies. Shape functions which satisfy available classical and nonclassical boundary conditions in nonlocal strain gradient theory are proposed. It is shown that the vibrational behavior of the nanoshell is influenced by the porosity volume fraction, porosity distribution, nonlocal coefficient, strain gradient coefficient, boundary conditions and radius-to-thickness ratio.

1 Introduction

Size-dependent modeling and analysis of micro/nanostructures can be performed using various nonclassical elasticity theories such as surface elasticity-, nonlocal and strain gradient-based theories [1–8]. Among them, the nonlocal elasticity theory of Eringen [9] is the most employed theory for static and dynamic analysis of nanobeams and nanoplates [10–19]. The simplest model of this theory introduces a scale parameter which results in a stiffness reduction mechanism. By defining this parameter, it is possible to consider wide-range interaction between atoms. Actually, bending rigidity of the nanostructure and their vibration frequencies and buckling loads are decreased by considering the nonlocal stress field effect. However, nonlocal elasticity theory is not able to consider strain gradient effects in modeling of nanostructures.

Nonlocal strain gradient calibration of nanostructures via experiments and molecular dynamic simulation shows that their mechanical characteristics can be described using two scale parameters [20–22]. In fact, these two scale parameters consider the stiffness-softening and stiffness-hardening effects due to nonlocal stress field and strain gradients on mechanical behavior of nanostructures.

Thus, the present author's works are mainly focused on analysis of nanobeams and nanoplates based on nonlocal strain gradient theory [23–26]. Application of nonlocal strain gradient theory for modeling and analysis of nanostructures is still at the beginning stage, and only few papers are published in this field [27–33].

In recent years, static and dynamic analyses of nanoshells have attracted the attention of several researchers. Zaera et al. [34] studied axisymmetric free vibration of closed thin spherical nanoshells based on nonlocal elasticity theory. Ke et al. [35] examined vibration behavior of cylindrical nanoshells under thermo-electrical fields and different boundary conditions using nonlocal elasticity theory. Rouhi et al. [36,37] studied vibration characteristics of cylindrical nanoshells with different shell theories based on surface elasticity theory. Mehralian

Mohammad Reza Barati (✉)
Aerospace Engineering Department, Center of Excellence in Computational Aerospace, Amirkabir University of Technology, Tehran, Iran
E-mail: mrb.barati@ymail.com; mrb.barati@aut.ac.ir

et al. [38] performed buckling analysis of piezoelectric cylindrical nanoshells with functionally graded material properties. Farajpour et al. [39] investigated free vibration and buckling behaviors of microtubules using piezoelectric nanoshells under electric voltage and thermal loading. Also, Sun et al. [40] performed buckling analysis of size-dependent cylindrical nanoshells with functionally graded material properties.

In the process of functionally graded material (FGM) fabrication, the existence of porosities and microvoids inside the materials possibly occurs due to technical problems. For example, shrinkages between adjacent compositions of metal and ceramic phases in FGMs can occur during the sintering process, which may lead to a number of porosities spreading inside the materials [41]. In addition, by using a multi-step sequential infiltration technique for producing FGMs, it was observed that the porosities appear mostly at the middle zone of the FGM specimens. This is because it is difficult to infiltrate the secondary material into the middle zone completely, while at the top and bottom zones, the process of material infiltration can be performed easier and leaves less porosity. Based on this information about porosities in FGMs, it is important to consider the porosity effect on dynamic behavior of engineering structures made of FGMs carrying porosities. Also, in the case of nanoscale beams and plates, porosities have a great influence on their mechanical characteristics, as shown by several researchers [42,43]. Literature review shows that there is no study on vibration of porous nanoshells based on nonlocal strain gradient theory.

In this research, free vibration analysis of FG nanoshells with porosities is carried out applying nonlocal strain gradient theory and first-order shell model. Two scale parameters are used to describe the size-dependent behavior of nanoshell. Even and uneven distributions of porosity have been considered. Material properties are dependent on the porosity volume fraction, and they are graded in the thickness direction according to power-law function. The governing equations are derived via Hamilton's principle, and vibration frequencies are obtained implementing Galerkin's technique. Based on the presented solution, it is possible to apply simply supported and clamped boundary conditions in the axial direction of NSGT cylindrical nanoshell. It is demonstrated that vibration frequencies of porous nanoshells are prominently affected by porosities volume fraction, porosity distribution, nonlocality, strain gradients and geometrical parameters.

2 Modeling of nanoshells based on NSGT

The stress field based on NSGT can be described as a contribution of a nonlocal stress $\sigma_{ij}^{(0)}$ and a higher-order stress field $\nabla\sigma_{ij}^{(1)}$ as [43]:

$$\sigma_{ij} = \sigma_{ij}^{(0)} - \nabla\sigma_{ij}^{(1)}, \tag{1}$$

where the stresses $\sigma_{ij}^{(0)}$ and $\sigma_{ij}^{(1)}$ are, respectively, related to strain ε_{ij} and strain gradient $\nabla\varepsilon_{ij}$ by [26,43]:

$$\sigma_{ij}^{(0)} = \int_V C_{ijkl}\alpha_0(x, x', e_0a)\varepsilon'_{kl}(x')dx', \tag{2a}$$

$$\sigma_{ij}^{(1)} = l^2\int_V C_{ijkl}\alpha_1(x, x', e_1a)\nabla\varepsilon'_{kl}(x')dx', \tag{2b}$$

where e_0a and e_1a are called lower- and higher-order nonlocal parameters; C_{ijkl} denotes the elastic coefficients. Also, $\alpha_0(x, x', e_0a)$ and $\alpha_1(x, x', e_1a)$ denote nonlocal Kernel functions. As discussed in previous investigations, selection of appropriate forms of these functions results in the following expression of constitutive equation for nonlocal strain gradient theory [26]:

$$[1-(e_1a)^2\nabla^2][1-(e_0a)^2\nabla^2]\sigma_{ij} = C_{ijkl}[1-(e_1a)^2\nabla^2]\varepsilon_{kl} - C_{ijkl}l^2[1-(e_0a)^2\nabla^2]\nabla^2\varepsilon_{kl} \tag{3}$$

in which ∇^2 denotes the Laplacian operator. For simplicity, supposing $e_1 = e_0 = e$ in Eq. (3) yields the following equation [24]:

$$[1-(ea)^2\nabla^2]\sigma_{ij} = C_{ijkl}[1-l^2\nabla^2]\varepsilon_{kl}. \tag{4}$$

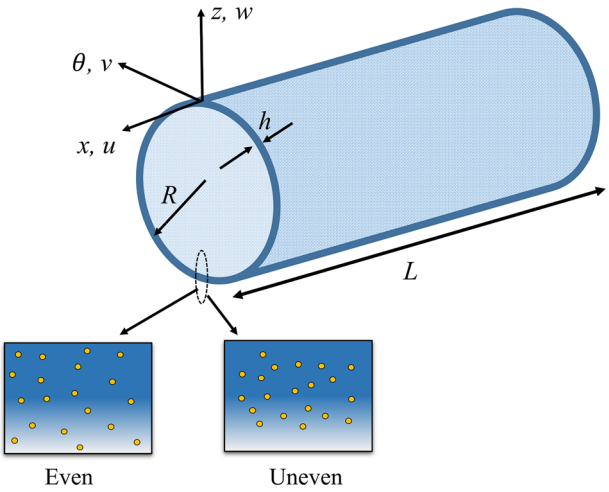

Fig. 1 Configuration of porous nanoshell with porosity distributions

3 Porous nanoshell model with different porosity distributions

Assume a porous nanoshell with thickness h as illustrated in Fig. 1. In the process of functionally graded material (FGM) fabrication, the existence of porosities and micro-voids inside the materials possibly occurs due to technical problems. For example, the shrinkages between adjacent compositions of metal and ceramic phases in FGMs can occur during the sintering process, which may lead to a number of porosities spreading inside the materials. In addition, by using multi-step sequential infiltration technique for producing FGMs, it was observed that the porosities appear mostly at the middle zone of the FGM specimens. This is because it is difficult to infiltrate the secondary material into the middle zone completely, while at the top and bottom zones, the process of material infiltration can be performed easier and leaves less porosity. Based on this information about porosities in FGMs, it is important to consider the porosity effect on dynamic behavior of engineering structures made of FGMs carrying porosities.

Two types of porosity distribution have been considered: (1) even distribution and (2) uneven distribution. In the case of even distribution, porosities are randomly distributed in the material structure. Moreover, in the case of uneven distribution, the porosities are distributed around the cross-sectional mid-zone and the amount of porosity diminishes at the top and bottom of the cross section.

The effective material properties of the porous FG nanoshell including Young's modulus (E) and density are variable across the thickness direction based on the modified power-law model as [42]:

$$E(z) = (E_c - E_m)\left(\frac{z}{h} + \frac{1}{2}\right)^p + E_m - (E_c + E_m)\frac{\xi}{2} \quad \text{for even porosities,} \tag{5a}$$

$$E(z) = (E_c - E_m)\left(\frac{z}{h} + \frac{1}{2}\right)^p + E_m - \frac{\xi}{2}(E_c + E_m)\left(1 - \frac{2|z|}{h}\right) \quad \text{for uneven porosities,} \tag{5b}$$

where p is the material gradation index and m and c are corresponding to the material properties of the top and bottom surfaces, respectively; ξ is the porosity volume fraction.

Assuming first-order shear deformation shell model, the displacement field of the nanoshell can be supposed as:

$$u_1(x, \theta, z, t) = u(x, \theta, t) + z\varphi_x(x, \theta, t), \tag{6a}$$

$$u_2(x, \theta, z, t) = v(x, \theta, t) + z\varphi_\theta(x, \theta, t), \tag{6b}$$

$$u_3(x, \theta, z, t) = w(x, \theta, t), \tag{6c}$$

where u, v and w are axial, circumferential and transverse displacements, respectively; φ_x and φ_θ are rotations about axial and circumferential axis.

It is now possible to obtain the strains based upon the present shell model as [22]:

$$\varepsilon_{xx} = \frac{\partial u}{\partial x} + z\frac{\partial \varphi_x}{\partial x},$$

$$\varepsilon_\theta = \frac{1}{R}(\frac{\partial v}{\partial \theta} + w + z\frac{\partial \varphi_\theta}{\partial \theta}),$$
$$\gamma_{x\theta} = \frac{1}{R}\frac{\partial u}{\partial \theta} + \frac{\partial v}{\partial x} + \frac{z}{R}\frac{\partial \varphi_x}{\partial \theta} + z\frac{\partial \varphi_\theta}{\partial x},$$
$$\gamma_{zx} = \varphi_x + \frac{\partial w}{\partial x}, \quad \gamma_{z\theta} = \varphi_\theta + \frac{1}{R}\frac{\partial w}{\partial \theta} - \frac{v}{R}. \tag{7}$$

Now, Hamilton's principle can be written as:

$$\int_0^t \delta(U - T - V)\mathrm{d}t = 0, \tag{8}$$

here, U is strain energy, T is kinetic energy, and V is work done by external forces and

$$\delta U = \int_V (\sigma_{ij}\delta\varepsilon_{ij} + \sigma_{ij}^{(1)}\delta\nabla\varepsilon_{ij})R\mathrm{d}x\mathrm{d}\theta\mathrm{d}z, \tag{9}$$
$$\delta V = \int_V \left(N_{r0} + N_{x0}\frac{\partial^2 w}{\partial x^2} + \frac{N_{\theta 0}}{R^2}\frac{\partial^2 w}{\partial \theta^2} + k_w + k_p\left(\frac{\partial^2 w}{\partial x^2} + \frac{1}{R^2}\frac{\partial^2 w}{\partial \theta^2}\right)\right)\delta w R\mathrm{d}x\mathrm{d}\theta\mathrm{d}z, \tag{10}$$
$$\delta K = \int_V \left(\left(\frac{\partial \delta u_1}{\partial t}\right)^2 + \left(\frac{\partial \delta u_2}{\partial t}\right)^2 + \left(\frac{\partial \delta u_3}{\partial t}\right)^2\right) R\mathrm{d}x\mathrm{d}\theta\mathrm{d}z, \tag{11}$$

in which σ_{ij}, $\sigma_{ij}^{(1)}$, $\varepsilon_{ij}$and $\nabla\varepsilon_{ij}$are defined in the previous chapter. Also, N_{r0}, $N_{x0}$and $N_{\theta 0}$ are radial, axial and torsional mechanical loads, respectively, which are discarded in this study. Also, k_w and k_p are Winkler and Pasternak foundation coefficients.

Using Hamilton's principle in Eq. (8) and Eqs. (9)–(11), the governing equations can be obtained as [22]:

$$\frac{\partial N_{xx}}{\partial x} + \frac{1}{R}\frac{\partial N_{x\theta}}{\partial \theta} = I_0\frac{\partial^2 u}{\partial t^2} + I_1\frac{\partial^2 \varphi_x}{\partial t^2}, \tag{12a}$$
$$\frac{\partial N_{x\theta}}{\partial x} + \frac{1}{R}\frac{\partial N_{\theta\theta}}{\partial \theta} + \frac{Q_{z\theta}}{R} = I_0\frac{\partial^2 v}{\partial t^2} + I_1\frac{\partial^2 \varphi_\theta}{\partial t^2}, \tag{12b}$$
$$\frac{\partial Q_{xz}}{\partial x} + \frac{1}{R}\frac{\partial Q_{z\theta}}{\partial \theta} - \frac{N_{\theta\theta}}{R} = + I_0\frac{\partial^2 w}{\partial t^2}, \tag{12c}$$
$$\frac{\partial M_{xx}}{\partial x} + \frac{1}{R}\frac{\partial M_{x\theta}}{\partial \theta} - Q_{xz} = I_1\frac{\partial^2 u}{\partial t^2} + I_2\frac{\partial^2 \varphi_x}{\partial t^2}, \tag{12d}$$
$$\frac{\partial M_{x\theta}}{\partial x} + \frac{1}{R}\frac{\partial M_{\theta\theta}}{\partial \theta} - Q_{\theta z} = I_1\frac{\partial^2 v}{\partial t^2} + I_2\frac{\partial^2 \varphi_\theta}{\partial t^2}, \tag{12e}$$

in which

$$(I_0, I_1, I_2) = \int_{-h/2}^{h/2}(1, z, z^2)\rho(z)\mathrm{d}z \tag{13}$$

and

$$\{N_{xx}, N_{\theta\theta}, N_{x\theta}\} = \int_{-h/2}^{h/2}\{\sigma_{xx}, \sigma_{\theta\theta}, \sigma_{x\theta}\}\mathrm{d}z, \tag{14a}$$
$$\{M_{xx}, M_{\theta\theta}, M_{x\theta}\} = \int_{-h/2}^{h/2}\{\sigma_{xx}, \sigma_{\theta\theta}, \sigma_{x\theta}\}z\mathrm{d}z, \tag{14b}$$
$$\{Q_{xz}, Q_{z\theta}\} = \kappa_s\int_{-h/2}^{h/2}\{\sigma_{xz}, \sigma_{z\theta}\}\mathrm{d}z, \tag{14c}$$

in which $\kappa_s = 5/6$ is the shear correction factor.

Based on the NSGT, the constitutive relations of the nanoshell can be stated as:

$$(1-\mu\nabla^2)\begin{Bmatrix}\sigma_{xx}\\ \sigma_{\theta\theta}\\ \sigma_{x\theta}\\ \sigma_{xz}\\ \sigma_{z\theta}\end{Bmatrix}=\frac{E(z)}{1-v^2}(1-\lambda\nabla^2)\begin{pmatrix}1 & v & 0 & 0 & 0\\ v & 1 & 0 & 0 & 0\\ 0 & 0 & (1-v)/2 & 0 & 0\\ 0 & 0 & 0 & (1-v)/2 & 0\\ 0 & 0 & 0 & 0 & (1-v)/2\end{pmatrix}\begin{Bmatrix}\varepsilon_{xx}\\ \varepsilon_{\theta\theta}\\ \gamma_{xy}\\ \gamma_{xz}\\ \gamma_{z\theta}\end{Bmatrix} \quad (15)$$

in which $\mu = ea/L$ and $\lambda = l/L$ are normalized nonlocal and strain gradient parameters, respectively. The nonlocal parameter ea consists of a characteristic internal length (a), for instance lattice parameter, C–C bond length and granular distance and a constant (e) dependent on each material. Usually, the value of e is experimentally estimated by comparing the scattering curves of plane waves and atomistic dynamics.

Integrating Eq. (15) over the nanoshell thickness, the resultants presented in Eqs. (14) can be obtained as presented in Appendix A.

The governing equations in terms of the displacements for a NSGT nanoshell can be derived by substituting Eqs. (A1)–(A8) into Eq. (12) as follows:

$$\begin{aligned}
&(1-\lambda\nabla^2)\left[A_{11}\frac{\partial^2 u}{\partial x^2}+B_{11}\frac{\partial^2\varphi_x}{\partial x^2}+\frac{A_{12}}{R}\left(\frac{\partial^2 v}{\partial x\partial\theta}+\frac{\partial w}{\partial x}\right)+\frac{B_{12}}{R}\frac{\partial^2\varphi_\theta}{\partial x\partial\theta}\right.\\
&\left.+\frac{A_{66}}{R}\left(\frac{1}{R}\frac{\partial^2 u}{\partial\theta^2}+\frac{\partial^2 v}{\partial x\partial\theta}\right)+\frac{B_{66}}{R}\left(\frac{1}{R}\frac{\partial^2\varphi_x}{\partial\theta^2}+\frac{\partial^2\varphi_\theta}{\partial x\partial\theta}\right)\right]+(1-\mu\nabla^2)\left[-I_0\frac{\partial^2 u}{\partial t^2}-I_1\frac{\partial^2\varphi_x}{\partial t^2}\right]=0, \quad (16a)\\
&(1-\lambda\nabla^2)\left[A_{66}\left(\frac{1}{R}\frac{\partial^2 u}{\partial x\partial\theta}+\frac{\partial^2 v}{\partial x^2}\right)+B_{66}\left(\frac{1}{R}\frac{\partial^2\varphi_x}{\partial x\partial\theta}+\frac{\partial^2\varphi_\theta}{\partial x^2}\right)\right.\\
&\frac{A_{12}}{R}\frac{\partial^2 u}{\partial x\partial\theta}+\frac{B_{12}}{R}\frac{\partial^2\varphi_x}{\partial x\partial\theta}+\frac{A_{11}}{R^2}\left(\frac{\partial^2 v}{\partial\theta^2}+\frac{\partial w}{\partial\theta}\right)+\frac{B_{11}}{R^2}\frac{\partial^2\varphi_\theta}{\partial\theta^2}\\
&\left.\frac{\tilde{A}_{66}}{R}\left(\varphi_\theta+\frac{1}{R}\frac{\partial w}{\partial\theta}-\frac{v}{R}\right)\right]+(1-\mu\nabla^2)\left[-I_0\frac{\partial^2 v}{\partial t^2}-I_1\frac{\partial^2\varphi_\theta}{\partial t^2}\right]=0, \quad (16b)\\
&(1-\lambda\nabla^2)\left[\tilde{A}_{66}\left(\frac{\partial\varphi_x}{\partial x}+\frac{\partial^2 w}{\partial x^2}\right)+\frac{\tilde{A}_{66}}{R}\left(\frac{\partial\varphi_\theta}{\partial\theta}+\frac{1}{R}\frac{\partial^2 w}{\partial\theta^2}-\frac{1}{R}\frac{\partial v}{\partial\theta}\right)\right.\\
&\left.-\frac{A_{12}}{R}\frac{\partial u}{\partial x}-\frac{B_{12}}{R}\frac{\partial\varphi_x}{\partial x}-\frac{A_{11}}{R^2}\left(\frac{\partial v}{\partial\theta}+w\right)-\frac{B_{11}}{R^2}\frac{\partial\varphi_\theta}{\partial\theta}\right]+(1-\mu\nabla^2)\left[-I_0\frac{\partial^2 w}{\partial t^2}\right]\\
&+(1-\mu\nabla^2)\left(-k_w w+k_p\left(\frac{\partial^2 w}{\partial x^2}+\frac{1}{R^2}\frac{\partial^2 w}{\partial\theta^2}\right)\right)=0, \quad (16c)\\
&(1-\lambda\nabla^2)\left[B_{11}\frac{\partial^2 u}{\partial x^2}+D_{11}\frac{\partial^2\varphi_x}{\partial x^2}+\frac{B_{12}}{R}\left(\frac{\partial^2 v}{\partial x\partial\theta}+\frac{\partial w}{\partial x}\right)+\frac{D_{12}}{R}\frac{\partial^2\varphi_\theta}{\partial x\partial\theta}\right.\\
&\frac{B_{66}}{R}\left(\frac{1}{R}\frac{\partial^2 u}{\partial\theta^2}+\frac{\partial^2 v}{\partial x\partial\theta}\right)+\frac{D_{66}}{R}\left(\frac{1}{R}\frac{\partial^2\varphi_x}{\partial\theta^2}+\frac{\partial^2\varphi_\theta}{\partial x\partial\theta}\right)-\tilde{A}_{66}\left(\varphi_x+\frac{\partial w}{\partial x}\right)\Big]\\
&+(1-\mu\nabla^2)\left[-I_1\frac{\partial^2 u}{\partial t^2}-I_2\frac{\partial^2\varphi_x}{\partial t^2}\right]=0, \quad (16d)\\
&(1-\lambda\nabla^2)\left[B_{66}\left(\frac{1}{R}\frac{\partial^2 u}{\partial x\partial\theta}+\frac{\partial^2 v}{\partial x^2}\right)+D_{66}\left(\frac{1}{R}\frac{\partial^2\varphi_x}{\partial x\partial\theta}+\frac{\partial^2\varphi_\theta}{\partial x^2}\right)\right.\\
&\frac{B_{12}}{R}\frac{\partial^2 u}{\partial x\partial\theta}+\frac{D_{12}}{R}\frac{\partial^2\varphi_x}{\partial x\partial\theta}+\frac{B_{11}}{R^2}\left(\frac{\partial^2 v}{\partial\theta^2}+\frac{\partial w}{\partial\theta}\right)+\frac{D_{11}}{R^2}\frac{\partial^2\varphi_\theta}{\partial\theta^2}\\
&\left.-\tilde{A}_{66}\left(\varphi_\theta+\frac{1}{R}\frac{\partial w}{\partial\theta}-\frac{v}{R}\right)\right]+(1-\mu\nabla^2)\left[-I_1\frac{\partial^2 v}{\partial t^2}-I_2\frac{\partial^2\varphi_\theta}{\partial t^2}\right]=0, \quad (16e)
\end{aligned}$$

in which:

$$A_{11}=\int_{-h/2}^{h/2}\frac{E(z)}{1-v^2}\mathrm{d}z,\quad B_{11}=\int_{-h/2}^{h/2}\frac{E(z)}{1-v^2}z\mathrm{d}z,\quad D_{11}=\int_{-h/2}^{h/2}\frac{E(z)z^2}{1-v^2}\mathrm{d}z,$$

$$A_{12}=\int_{-h/2}^{h/2}\frac{vE(z)}{1-v^2}\mathrm{d}z,\quad B_{12}=\int_{-h/2}^{h/2}\frac{vE(z)}{1-v^2}z\mathrm{d}z,\quad D_{12}=\int_{-h/2}^{h/2}\frac{vE(z)z^2}{1-v^2}\mathrm{d}z,$$
$$A_{66}=\int_{-h/2}^{h/2}\frac{E(z)}{2(1+v)}\mathrm{d}z,\quad B_{66}=\int_{-h/2}^{h/2}\frac{E(z)}{2(1+v)}z\mathrm{d}z,\quad D_{66}=\int_{-h/2}^{h/2}\frac{E(z)}{2(1+v)}z^2\mathrm{d}z,$$
$$\tilde{A}_{66}=k_s\int_{-h/2}^{h/2}\frac{E(z)}{2(1+v)}\mathrm{d}z. \tag{17}$$

4 Solution procedure

In this section, Galerkin's method is implemented to solve the governing equations of nonlocal strain gradient porous nanoshells. Thus, the displacement field can be calculated as:

$$u=\sum_{m=1}^{\infty}\sum_{n=1}^{\infty}U_{mn}\frac{\partial X_m(x)}{\partial x}\cos(n\theta)\,e^{i\omega_n t}, \tag{18}$$
$$v=\sum_{m=1}^{\infty}\sum_{n=1}^{\infty}V_{mn}X_m(x)\sin(n\theta)\,e^{i\omega_n t}, \tag{19}$$
$$w=\sum_{m=1}^{\infty}\sum_{n=1}^{\infty}W_{mn}X_m(x)\cos(n\theta)\,e^{i\omega_n t}, \tag{20}$$
$$\varphi_x=\sum_{m=1}^{\infty}\sum_{n=1}^{\infty}\Phi_{mn}\frac{\partial X_m(x)}{\partial x}\cos(n\theta)\,e^{i\omega_n t}, \tag{21}$$
$$\varphi_\theta=\sum_{m=1}^{\infty}\sum_{n=1}^{\infty}\Theta_{mn}X_m(x)\sin(n\theta)\,e^{i\omega_n t}, \tag{22}$$

where $(U_{mn}, V_{mn}, W_{mn}, \Phi_{mn}, \Theta_{mn})$ are the unknown coefficients and the function X_m satisfies the boundary conditions in x-direction. The classical and nonclassical boundary conditions at $x = 0, L$ can be represented by:

Simply supported–simply supported (S–S)

$$w=0 \text{ geometric boundary condition}$$
$$\frac{\partial^2 w}{\partial x^2}=\frac{\partial^4 w}{\partial x^4}=0 \text{ force boundary conditions} \tag{23a}$$

Clamped–clamped (C–C)

$$w=\frac{\partial w}{\partial x}=0 \text{ geometric boundary conditions}$$
$$\frac{\partial^3 w}{\partial x^3}=0 \text{ force boundary condition} \tag{23b}$$

By substituting Eqs. (18)–(22) into Eqs. (16) and using the Galerkin's method, one obtains

$$\left\{[K]+\omega_n^2[M]\right\}\begin{Bmatrix}U_{mn}\\V_{mn}\\W_{mn}\\\Phi_{mn}\\\Theta_{mn}\end{Bmatrix}=0 \tag{24}$$

in which ω_n is the natural frequency. The components of mass and stiffness matrices are presented in Appendix B. Also, nondimensional parameters are defined as:

$$\varpi=100\omega_n h\sqrt{\frac{\rho_c}{E_c}},\quad K_w=\frac{k_w L^4}{D_2},\quad K_p=\frac{k_p L^2}{D_2},$$

Table 1 Comparison of natural frequencies of size-dependent nanoshells

L/2R	MD (Mehralian et al. [22])	NSGT (Mehralian et al. [22])	Present
4.86	1.138	1.209	1.208
8.47	0.466	0.448	0.447
13.89	0.190	0.192	0.193
17.47	0.122	0.126	0.126

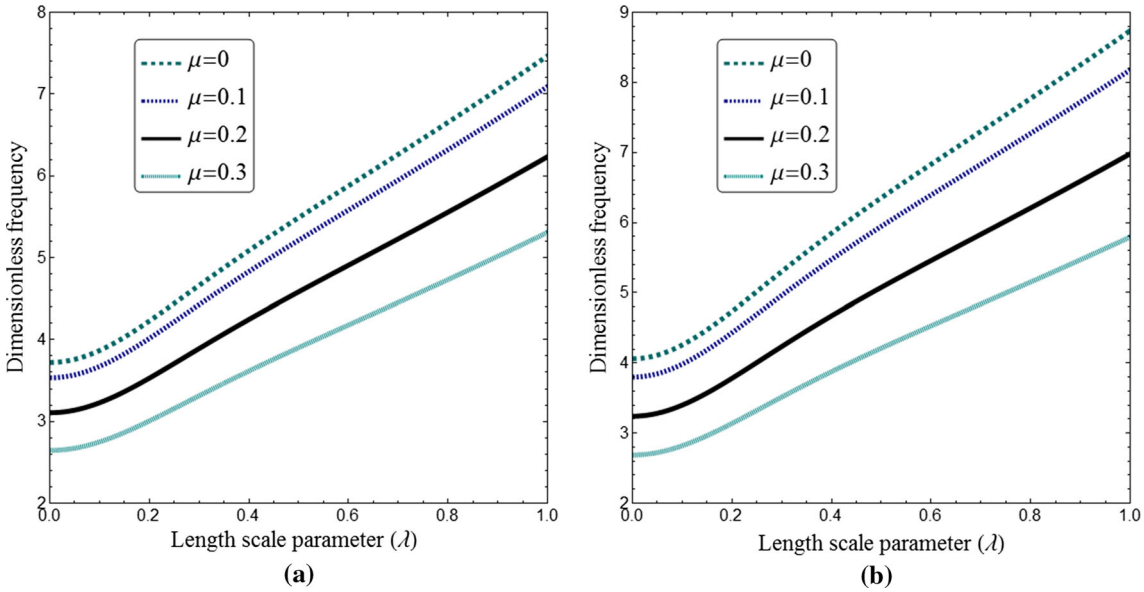

Fig. 2 Variation of dimensionless frequency of the nanoshell versus length scale parameter for various nonlocal parameters ($R/h = 20$, $p = 1, \xi = 0$)

$$D_2 = \frac{E_c h^3}{12(1-v^2)}, \quad \mu = \frac{ea}{L}, \quad \lambda = \frac{l}{L}. \tag{25}$$

Finally, setting the coefficient matrix to zero gives the natural frequencies. The function X_m for considered boundary conditions is defined by:

$$X_m(x) = \sin\left(\frac{m\pi}{L}x\right) \text{ for S–S}, \tag{26}$$

$$X_m(x) = \sin^2\left(\frac{m\pi}{L}x\right) \text{ for C–C}. \tag{27}$$

It is clear that above functions satisfy boundary conditions presented in Eq. (23) at $x = 0, L$.

5 Numerical results and discussion

This section studies free vibrational behavior of porous functionally graded (FG) nanoshells using nonlocal strain gradient theory (NSGT). A nonlocal parameter and a strain gradient parameter are employed to describe both stiffness reduction and stiffness enhancement of nanoshells. Porosities are evenly and unevenly distributed through the thickness of the nanoshell. In Table 1, vibration frequencies of nanoshells based on first-order shell model and nonlocal strain gradient theory are compared with those reported by Mehralian et al. [22] using molecular dynamic simulation. For comparison, varying nonlocal parameter $\mu = 3.3 - 3.5\,\text{nm}^2$ and strain gradient parameter $\lambda = 0.1 - 0.4\,\text{nm}^2$ are considered. Results are in excellent agreement with those of Mehralian et al. [22]. In the present study, the material properties of FG nanoshell are considered as:

- $E_c = 380\,\text{GPa}, \quad \rho_c = 3800\,\text{kg/m}^3, \quad v_c = 0.3$
- $E_m = 70\,\text{GPa}, \quad \rho_m = 2707\,\text{kg/m}^3, \quad v_m = 0.3$

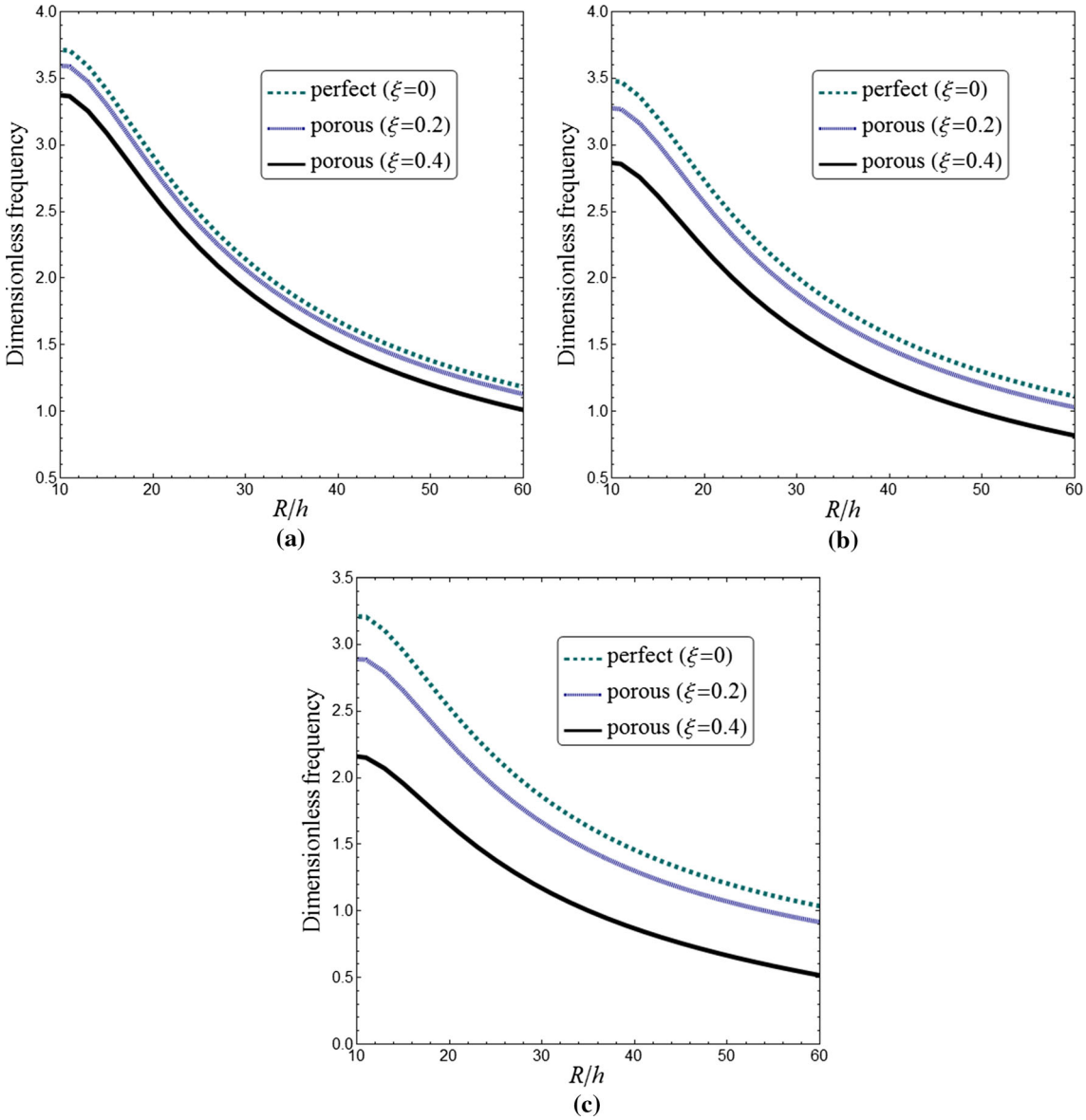

Fig. 3 Variation of dimensionless frequency of the nanoshell versus radius-to-thickness ratio for various porosity volume fractions ($L/h = 20$, $\mu = 0.2$, $\lambda = 0.1$)

Figure 2 examines the effects of nonlocal and strain gradient parameters on nondimensional vibration frequency of FG nanoshells with S–S and C–C boundary conditions when $R/h = 20$, $p = 1$ and $\xi = 0$. It is possible to obtain the frequency results of nonlocal elasticity theory without strain gradients by setting λ=0. Based on NSGT, increasing strain gradient parameter results in larger vibration frequency for every value of nonlocal parameter. This observation highlights the stiffness enhancement effect by considering strain gradients. However, vibration frequencies become smaller with the rise of nonlocal parameter showing stiffness reduction influence due to nonlocal stress field. The above discussion reveals that both nonlocal and strain gradient parameters should be considered for modeling of nanoshells. In fact, by neglecting strain gradient effect, the influence of microstructural behavior has been discarded. These observations are valid for both S-S and C-C nanoshells.

Influences of porosity volume fraction and material gradient index on vibration frequency of FG nanoshell with respect to radius-to-thickness ratio (R/h) are shown in Fig. 3 at $L/h = 20$, $\mu = 0.2$, $\lambda = 0.1$. It is clear that a porous nanoshell has lower natural frequencies than a perfect nanoshell ($\xi = 0$). In other words,

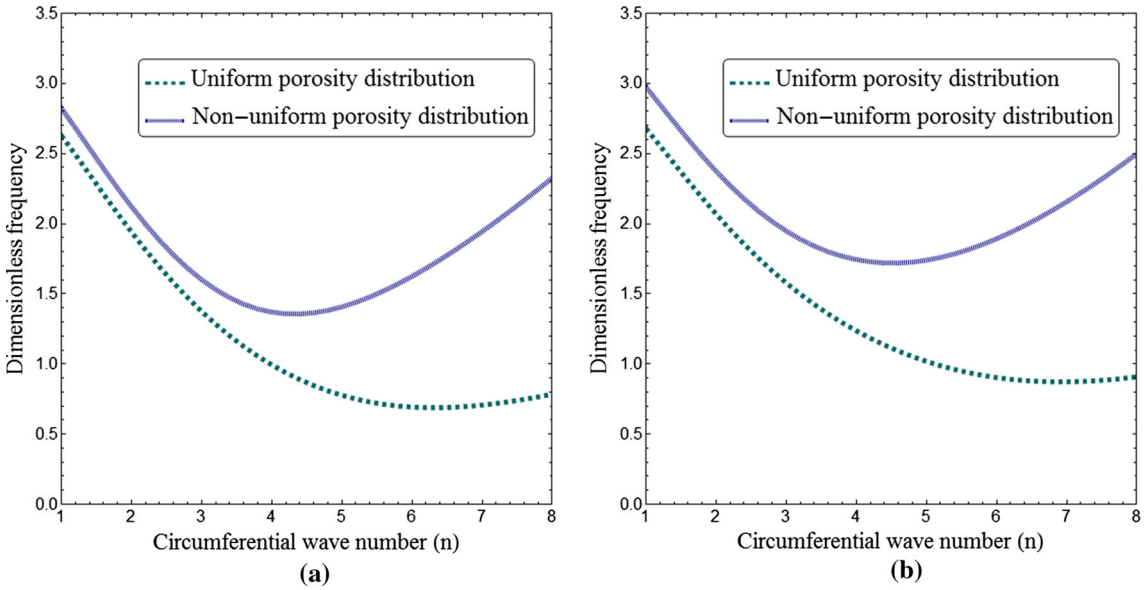

Fig. 4 Variation of dimensionless frequency of the nanoshell versus circumferential wave number for different porosity distributions ($R/h = 20$, $p = 2$, $\xi = 0.4$)

increasing porosity volume fraction results in smaller natural frequencies due to the reduction in the bending rigidity of the nanoshell. Therefore, for better understanding of the mechanical behavior of nanoshells, it is crucial to consider porosities inside the material structure. However, vibration frequencies reduce with increasing material gradient index (p) due to the higher portion of metal phase at larger gradient indices. One can also see that vibration frequencies are significantly decreased with the increase in radius-to-thickness ratio. This is because nanoshells with higher radius-to-thickness ratios are more flexible leading to smaller vibration frequencies.

The effect of porosity distribution on the natural frequency of porous nanoshells with respect to the circumferential wave number (n) is shown in Fig. 4 at $R/h = 20$, $p = 2$ and $\xi = 0.4$. It can be observed that uneven (nonuniform) porosity distribution provides larger vibration frequencies than uniform or even porosity distribution. This is due to the fact that in the uneven model, porosities vanished at the top and bottom sides of the nanoshell thickness. Therefore, uneven porosity distribution gives better mechanical performance for porous nanoshells. Also, porosity distribution effect is significantly affected by the circumferential wave number. Generally, the vibration frequency first decreases and then increases with an increase in the circumferential wave number. However, the effect of porosity distribution becomes more significant at higher wave numbers.

Figure 5 indicates the effect of length-to-thickness ratio (L/h) of the nanoshell for different Winkler and Pasternak foundation parameters when $\xi = 0.2$, $\mu = 0.2$ and $\lambda = 0.1$. A simply supported–simply supported nanoshell with even porosities has been considered in this figure. Similar to the radius-to-thickness ratio (R/h), increasing L/h results in a more flexible nanoshell and smaller vibration frequencies. But, higher values of Winkler and Pasternak foundation constants yield an increase in the bending rigidity and natural frequency of the nanoshell. However, the surrounding shear layer (K_p) has a continuous interaction with the nanoshell and its effect on vibration frequency is more sensible than the Winkler layer.

6 Conclusions

In this paper, the free vibration behavior of nonlocal strain gradient porous shells in an elastic medium was explored by employing a first-order shell model. Even and uneven porosity distributions were considered. Two scale coefficients were considered for a better size-dependent modeling of the nanoshell. It was observed that increasing the nonlocal parameter results in reduction in the vibration frequencies. However, an inverse trend was observed when considering strain gradient effects. An increase in porosity volume fraction gave smaller natural frequencies. However, uneven porosity distribution provided larger frequencies compared with even

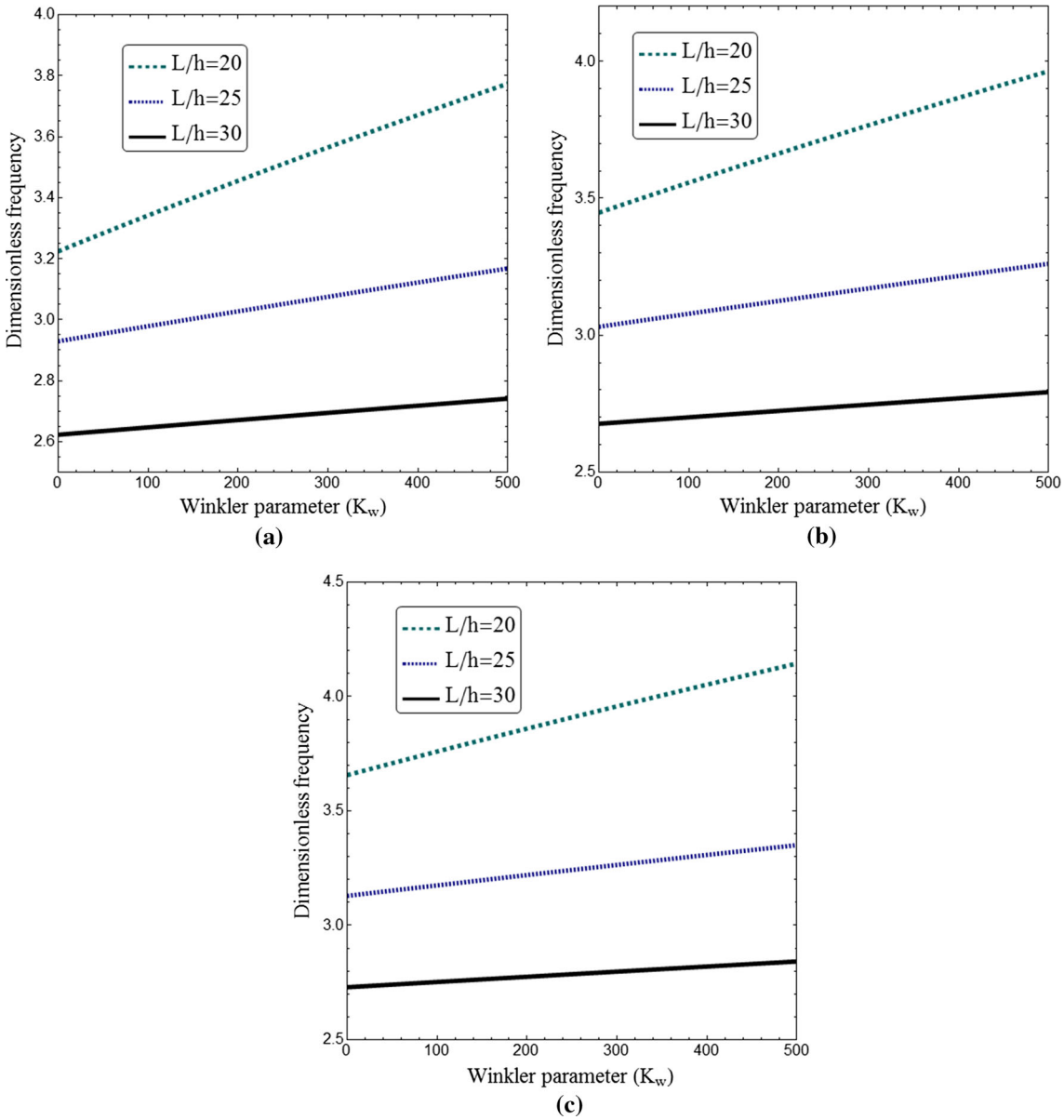

Fig. 5 Variation of dimensionless frequency of the nanoshell versus Winkler parameter for various length-to-thickness ratios ($\xi = 0.2$, $\mu = 0.2$, $\lambda = 0.1$)

porosity distribution. Increasing the length-to-thickness and radius-to-thickness ratios led to a more flexible nanoshell and smaller frequencies, while increasing the foundation coefficients gave larger frequencies.

Appendix A

$$\left(1-\mu\nabla^2\right)N_{xx} = \left(1-\lambda\nabla^2\right)\left[A_{11}\frac{\partial u}{\partial x} + B_{11}\frac{\partial \varphi_x}{\partial x} + \frac{A_{12}}{R}\left(\frac{\partial v}{\partial \theta} + w\right) + \frac{B_{12}}{R}\frac{\partial \varphi_\theta}{\partial \theta}\right] \tag{A1}$$

$$\left(1-\mu\nabla^2\right)M_{xx} = \left(1-\lambda\nabla^2\right)\left[B_{11}\frac{\partial u}{\partial x} + D_{11}\frac{\partial \varphi_x}{\partial x} + \frac{B_{12}}{R}\left(\frac{\partial v}{\partial \theta} + w\right) + \frac{D_{12}}{R}\frac{\partial \varphi_\theta}{\partial \theta}\right] \tag{A2}$$

$$\left(1-\mu\nabla^2\right)N_{\theta\theta}=\left(1-\lambda\nabla^2\right)\left[A_{12}\frac{\partial u}{\partial x}+B_{12}\frac{\partial\varphi_x}{\partial x}+\frac{A_{11}}{R}\left(\frac{\partial v}{\partial\theta}+w\right)+\frac{B_{11}}{R}\frac{\partial\varphi_\theta}{\partial\theta}\right] \tag{A3}$$

$$\left(1-\mu\nabla^2\right)M_{\theta\theta}=\left(1-\lambda\nabla^2\right)\left[B_{12}\frac{\partial u}{\partial x}+D_{12}\frac{\partial\varphi_x}{\partial x}+\frac{B_{11}}{R}\left(\frac{\partial v}{\partial\theta}+w\right)+\frac{D_{11}}{R}\frac{\partial\varphi_\theta}{\partial\theta}\right] \tag{A4}$$

$$\left(1-\mu\nabla^2\right)N_{x\theta}=\left(1-\lambda\nabla^2\right)\left[A_{66}\left(\frac{1}{R}\frac{\partial u}{\partial\theta}+\frac{\partial v}{\partial x}\right)+B_{66}\left(\frac{1}{R}\frac{\partial\varphi_x}{\partial\theta}+\frac{\partial\varphi_\theta}{\partial x}\right)\right] \tag{A5}$$

$$\left(1-\mu\nabla^2\right)M_{x\theta}=\left(1-\lambda\nabla^2\right)\left[B_{66}\left(\frac{1}{R}\frac{\partial u}{\partial\theta}+\frac{\partial v}{\partial x}\right)+D_{66}\left(\frac{1}{R}\frac{\partial\varphi_x}{\partial\theta}+\frac{\partial\varphi_\theta}{\partial x}\right)\right] \tag{A6}$$

$$\left(1-\mu\nabla^2\right)Q_{xz}=\left(1-\lambda\nabla^2\right)\tilde{A}_{66}\left(\varphi_x+\frac{\partial w}{\partial x}\right) \tag{A7}$$

$$\left(1-\mu\nabla^2\right)Q_{\theta z}=\left(1-\lambda\nabla^2\right)\tilde{A}_{66}\left(\varphi_\theta+\frac{1}{R}\frac{\partial w}{\partial\theta}-\frac{v}{R}\right) \tag{A8}$$

Appendix B

$$k_{1,1}=A_{11}\left(\Upsilon_{31}-\lambda\left(\Upsilon_{51}-\frac{n^2}{R}\Upsilon_{31}\right)\right)-n^2\frac{A_{66}}{R^2}\left(\Upsilon_{11}-\lambda\left(\Upsilon_{31}-\frac{n^2}{R}\Upsilon_{11}\right)\right) \tag{B1}$$

$$k_{2,1}=n\left(\frac{A_{12}}{R}+\frac{A_{66}}{R}\right)\left(\Upsilon_{11}-\lambda\left(\Upsilon_{31}-\frac{n^2}{R}\Upsilon_{11}\right)\right)$$

$$k_{1,2}=-n\left(\frac{A_{12}}{R}+\frac{A_{66}}{R}\right)\left(\Upsilon_{20}-\lambda\left(\Upsilon_{40}-\frac{n^2}{R}\Upsilon_{20}\right)\right) \tag{B2}$$

$$k_{3,1}=+\frac{A_{12}}{R}\left(\Upsilon_{11}-\lambda\left(\Upsilon_{31}-\frac{n^2}{R}\Upsilon_{11}\right)\right)$$

$$k_{1,3}=-\frac{A_{12}}{R}\left(\Upsilon_{20}-\lambda\left(\Upsilon_{40}-\frac{n^2}{R}\Upsilon_{20}\right)\right) \tag{B3}$$

$$k_{4,1}=+B_{11}\left(\Upsilon_{31}-\lambda\left(\Upsilon_{51}-\frac{n^2}{R}\Upsilon_{31}\right)\right)-n^2\frac{B_{66}}{R^2}\left(\Upsilon_{11}-\lambda\left(\Upsilon_{31}-\frac{n^2}{R}\Upsilon_{11}\right)\right) \tag{B4}$$

$$k_{1,4}=B_{11}\left(\Upsilon_{31}-\lambda\left(\Upsilon_{51}-\frac{n^2}{R}\Upsilon_{31}\right)\right)-n^2\frac{B_{66}}{R^2}\left(\Upsilon_{11}-\lambda\left(\Upsilon_{31}-\frac{n^2}{R}\Upsilon_{11}\right)\right) \tag{B5}$$

$$k_{5,1}=n\left(\frac{B_{12}}{R}+\frac{B_{66}}{R}\right)\left(\Upsilon_{11}-\lambda\left(\Upsilon_{31}-\frac{n^2}{R}\Upsilon_{11}\right)\right)$$

$$k_{1,5}=-n\left(\frac{B_{66}}{R}+\frac{B_{12}}{R}\right)\left(\Upsilon_{20}-\lambda\left(\Upsilon_{40}-\frac{n^2}{R}\Upsilon_{20}\right)\right) \tag{B6}$$

$$k_{2,2}=A_{66}\left(\Upsilon_{20}-\lambda\left(\Upsilon_{40}-\frac{n^2}{R}\Upsilon_{20}\right)\right)-n^2\frac{A_{11}}{R^2}\left(\Upsilon_{00}-\lambda\left(\Upsilon_{20}-\frac{n^2}{R}\Upsilon_{00}\right)\right)$$
$$-\frac{\tilde{A}_{66}}{R^2}\left(\Upsilon_{00}-\lambda\left(\Upsilon_{20}-\frac{n^2}{R}\Upsilon_{00}\right)\right) \tag{B7}$$

$$k_{3,2}=-n\left(\frac{A_{11}}{R^2}+\frac{\tilde{A}_{66}}{R^2}\right)\left(\Upsilon_{00}-\lambda\left(\Upsilon_{20}-\frac{n^2}{R}\Upsilon_{00}\right)\right)$$

$$k_{2,3}=-n\left(\frac{\tilde{A}_{66}}{R^2}+\frac{A_{11}}{R^2}\right)\left(\Upsilon_{00}-\lambda\left(\Upsilon_{20}-\frac{n^2}{R}\Upsilon_{00}\right)\right) \tag{B8}$$

$$k_{4,2}=-n\left(\frac{B_{12}}{R}+\frac{B_{66}}{R}\right)\left(\Upsilon_{20}-\lambda\left(\Upsilon_{40}-\frac{n^2}{R}\Upsilon_{20}\right)\right)$$

$$k_{2,4} = +n\left(\frac{B_{12}}{R}+\frac{B_{66}}{R}\right)\left(\Upsilon_{11}-\lambda\left(\Upsilon_{31}-\frac{n^2}{R}\Upsilon_{11}\right)\right) \tag{B9}$$

$$k_{5,2} = B_{66}\left(\Upsilon_{20}-\lambda\left(\Upsilon_{40}-\frac{n^2}{R}\Upsilon_{20}\right)\right)-n^2\frac{B_{11}}{R^2}\left(\Upsilon_{00}-\lambda\left(\Upsilon_{20}-\frac{n^2}{R}\Upsilon_{00}\right)\right) + \frac{\tilde{A}_{66}}{R}\left(\Upsilon_{00}-\lambda\left(\Upsilon_{20}-\frac{n^2}{R}\Upsilon_{00}\right)\right) \tag{B10}$$

$$\begin{aligned} k_{3,3} = {} & \tilde{A}_{66}\left(\Upsilon_{20}-\lambda\left(\Upsilon_{40}-\frac{n^2}{R}\Upsilon_{20}\right)\right)-n^2\frac{\tilde{A}_{66}}{R^2}\left(\Upsilon_{00}-\lambda\left(\Upsilon_{20}-\frac{n^2}{R}\Upsilon_{00}\right)\right) \\ & -\frac{A_{11}}{R^2}\left(\Upsilon_{00}-\lambda\left(\Upsilon_{20}-\frac{n^2}{R}\Upsilon_{00}\right)\right) \\ & -k_w\left(\Upsilon_{00}-\mu\left(\Upsilon_{20}-\frac{n^2}{R}\Upsilon_{00}\right)\right)+k_p\left(\left(\Upsilon_{20}-\mu\left(\Upsilon_{40}-\frac{n^2}{R}\Upsilon_{20}\right)\right)\right. \\ & \left.-\frac{n^2}{R}\left(\Upsilon_{00}-\mu\left(\Upsilon_{20}-\frac{n^2}{R}\Upsilon_{00}\right)\right)\right) \end{aligned} \tag{B11}$$

$$k_{4,3} = \left(\tilde{A}_{66}-\frac{B_{12}}{R}\right)\left(\Upsilon_{20}-\lambda\left(\Upsilon_{40}-\frac{n^2}{R}\Upsilon_{20}\right)\right)$$

$$k_{3,4} = +\left(\frac{B_{12}}{R}-\tilde{A}_{66}\right)\left(\Upsilon_{11}-\lambda\left(\Upsilon_{31}-\frac{n^2}{R}\Upsilon_{11}\right)\right) \tag{B12}$$

$$k_{5,3} = n\left(+\frac{\tilde{A}_{66}}{R}-\frac{B_{11}}{R^2}\right)\left(\Upsilon_{00}-\lambda\left(\Upsilon_{20}-\frac{n^2}{R}\Upsilon_{00}\right)\right)$$

$$k_{3,5} = -n\left(+\frac{B_{11}}{R^2}-\frac{\tilde{A}_{66}}{R}\right)\left(\Upsilon_{00}-\lambda\left(\Upsilon_{20}-\frac{n^2}{R}\Upsilon_{00}\right)\right) \tag{B13}$$

$$\begin{aligned} k_{4,4} = {} & +D_{11}\left(\Upsilon_{31}-\lambda\left(\Upsilon_{51}-\frac{n^2}{R}\Upsilon_{31}\right)\right)-n^2\frac{D_{66}}{R^2}\left(\Upsilon_{11}-\lambda\left(\Upsilon_{31}-\frac{n^2}{R}\Upsilon_{11}\right)\right) \\ & -\tilde{A}_{66}\left(\Upsilon_{11}-\lambda\left(\Upsilon_{31}-\frac{n^2}{R}\Upsilon_{11}\right)\right) \end{aligned} \tag{B14}$$

$$k_{5,4} = +n\left(\frac{D_{12}}{R}+\frac{D_{66}}{R}\right)\left(\Upsilon_{11}-\lambda\left(\Upsilon_{31}-\frac{n^2}{R}\Upsilon_{11}\right)\right)$$

$$k_{4,5} = -n\left(\frac{D_{66}}{R}+\frac{D_{12}}{R}\right)\left(\Upsilon_{20}-\lambda\left(\Upsilon_{40}-\frac{n^2}{R}\Upsilon_{20}\right)\right) \tag{B15}$$

$$\begin{aligned} k_{5,5} = {} & +D_{66}\left(\Upsilon_{20}-\lambda\left(\Upsilon_{40}-\frac{n^2}{R}\Upsilon_{20}\right)\right)-n^2\frac{D_{11}}{R^2}\left(\Upsilon_{00}-\lambda\left(\Upsilon_{20}-\frac{n^2}{R}\Upsilon_{00}\right)\right) \\ & -\tilde{A}_{66}\left(\Upsilon_{00}-\lambda\left(\Upsilon_{20}-\frac{n^2}{R}\Upsilon_{00}\right)\right) \end{aligned} \tag{B16}$$

$$m_{1,1} = +I_0\left(\Upsilon_{11}-\mu\left(\Upsilon_{30}-\frac{n^2}{R}\Upsilon_{11}\right)\right) \tag{B17}$$

$$m_{2,2} = m_{3,3} = m_{5,5} = +I_0\left(\Upsilon_{00}-\mu\left(\Upsilon_{20}-\frac{n^2}{R}\Upsilon_{00}\right)\right) \tag{B18}$$

$$m_{4,4} = +I_2\left(\Upsilon_{11}-\mu\left(\Upsilon_{30}-\frac{n^2}{R}\Upsilon_{11}\right)\right) \tag{B19}$$

$$m_{4,1} = +I_1\left(\Upsilon_{11}-\mu\left(\Upsilon_{30}-\frac{n^2}{R}\Upsilon_{11}\right)\right) \tag{B20}$$

$$m_{5,2} = m_{2,5} = +I_1\left(\Upsilon_{00} - \mu\left(\Upsilon_{20} - \frac{n^2}{R}\Upsilon_{00}\right)\right) \tag{B21}$$

where

$$\Upsilon_{00} = \int_0^L X_m X_m \mathrm{d}x \tag{B22}$$

$$\Upsilon_{20} = \int_0^L \frac{\mathrm{d}^2 X_m}{\mathrm{d}x^2} X_m \mathrm{d}x \tag{B23}$$

$$\Upsilon_{11} = \int_0^L \frac{\mathrm{d}X_m}{\mathrm{d}x}\frac{\mathrm{d}X_m}{\mathrm{d}x}\mathrm{d}x \tag{B24}$$

$$\Upsilon_{31} = \int_0^L \frac{\mathrm{d}^3 X_m}{\mathrm{d}x^3}\frac{\mathrm{d}X_m}{\mathrm{d}x}\mathrm{d}x \tag{B25}$$

$$\Upsilon_{40} = \int_0^L \frac{\mathrm{d}^4 X_m}{\mathrm{d}x^4} X_m \mathrm{d}x \tag{B26}$$

References

1. Aydogdu, M.: A general nonlocal beam theory: its application to nanobeam bending, buckling and vibration. Phys. E Low Dimens. Syst. Nanostruct. **41**(9), 1651–1655 (2009)
2. Thai, H.T.: A nonlocal beam theory for bending, buckling, and vibration of nanobeams. Int. J. Eng. Sci. **52**, 56–64 (2012)
3. Ke, L.L., Wang, Y.S., Wang, Z.D.: Nonlinear vibration of the piezoelectric nanobeams based on the nonlocal theory. Compos. Struct. **94**(6), 2038–2047 (2012)
4. Sharabiani, P.A., Yazdi, M.R.H.: Nonlinear free vibrations of functionally graded nanobeams with surface effects. Compos. B Eng. **45**(1), 581–586 (2013)
5. Eltaher, M.A., Mahmoud, F.F., Assie, A.E., Meletis, E.I.: Coupling effects of nonlocal and surface energy on vibration analysis of nanobeams. Appl. Math. Comput. **224**, 760–774 (2013)
6. Malekzadeh, P., Shojaee, M.: Surface and nonlocal effects on the nonlinear free vibration of non-uniform nanobeams. Compos. B Eng. **52**, 84–92 (2013)
7. Miandoab, E.M., Pishkenari, H.N., Yousefi-Koma, A., Hoorzad, H.: Polysilicon nano-beam model based on modified couple stress and Eringen's nonlocal elasticity theories. Phys. E Low Dimens. Syst. Nanostruct. **63**, 223–228 (2014)
8. Khorshidi, M.A., Shariati, M., Emam, S.A.: Postbuckling of functionally graded nanobeams based on modified couple stress theory under general beam theory. Int. J. Mech. Sci. **110**, 160–169 (2016)
9. Eringen, A.C.: On differential equations of nonlocal elasticity and solutions of screw dislocation and surface waves. J. Appl. Phys. **54**(9), 4703–4710 (1983)
10. Mohammadi, M., Safarabadi, M., Rastgoo, A., Farajpour, A.: Hygro-mechanical vibration analysis of a rotating viscoelastic nanobeam embedded in a visco-Pasternak elastic medium and in a nonlinear thermal environment. Acta Mech. **227**(8), 2207–2232 (2016)
11. Hosseini-Hashemi, S., Nahas, I., Fakher, M., Nazemnezhad, R.: Surface effects on free vibration of piezoelectric functionally graded nanobeams using nonlocal elasticity. Acta Mech. **225**(6), 1555 (2014)
12. Arefi, M., Zenkour, A.M.: Transient sinusoidal shear deformation formulation of a size-dependent three-layer piezo-magnetic curved nanobeam. Acta Mech. **228**, 1–18 (2017)
13. Rajabi, K., Hosseini-Hashemi, S.: Application of the generalized Hooke's law for viscoelastic materials (GHVMs) in nonlocal free damped vibration analysis of viscoelastic orthotropic nanoplates. Int. J. Mech. Sci. **124**, 158–165 (2017)
14. Zenkour, A.M., Abouelregal, A.E.: Vibration of FG nanobeams induced by sinusoidal pulse-heating via a nonlocal thermoelastic model. Acta Mech. **225**(12), 3409–3421 (2014)
15. Ebrahimi, F., Barati, M.R.: Vibration analysis of viscoelastic inhomogeneous nanobeams resting on a viscoelastic foundation based on nonlocal strain gradient theory incorporating surface and thermal effects. Acta Mech. **228**(3), 1197–1210 (2017)
16. Barati, M.R., Shahverdi, H.: An analytical solution for thermal vibration of compositionally graded nanoplates with arbitrary boundary conditions based on physical neutral surface position. Mech. Adv. Mater. Struct. **24**(10), 840–853 (2017)
17. Ebrahimi, F., Barati, M.R.: Size-dependent thermal stability analysis of graded piezomagnetic nanoplates on elastic medium subjected to various thermal environments. Appl. Phys. A **122**(10), 910 (2016)
18. Barati, M.R., Shahverdi, H.: A four-variable plate theory for thermal vibration of embedded FG nanoplates under non-uniform temperature distributions with different boundary conditions. Struct. Eng. Mech. **60**(4), 707–727 (2016)
19. Barati, M.R., Zenkour, A.M., Shahverdi, H.: Thermo-mechanical buckling analysis of embedded nanosize FG plates in thermal environments via an inverse cotangential theory. Compos. Struct. **141**, 203–212 (2016)
20. Lim, C.W., Zhang, G., Reddy, J.N.: A higher-order nonlocal elasticity and strain gradient theory and its applications in wave propagation. J. Mech. Phys. Solids **78**, 298–313 (2015)
21. Li, L., Hu, Y., Ling, L.: Wave propagation in viscoelastic single-walled carbon nanotubes with surface effect under magnetic field based on nonlocal strain gradient theory. Phys. E Low Dimens. Syst. Nanostruct. **75**, 118–124 (2016)
22. Mehralian, F., Beni, Y.T., Zeverdejani, M.K.: Nonlocal strain gradient theory calibration using molecular dynamics simulation based on small scale vibration of nanotubes. Phys. B Condens. Matter **514**, 61–69 (2017)

23. Ebrahimi, F., Barati, M.R., Dabbagh, A.: A nonlocal strain gradient theory for wave propagation analysis in temperature-dependent inhomogeneous nanoplates. Int. J. Eng. Sci. **107**, 169–182 (2016)
24. Barati, M.R., Shahverdi, H.: Hygro-thermal vibration analysis of graded double-refined-nanoplate systems using hybrid nonlocal stress–strain gradient theory. Compos. Struct. **176**, 982–995 (2017)
25. Ebrahimi, F., Barati, M.R.: A nonlocal strain gradient refined beam model for buckling analysis of size-dependent shear-deformable curved FG nanobeams. Compos. Struct. **159**, 174–182 (2017)
26. Barati, M.R., Zenkour, A.: A general bi-Helmholtz nonlocal strain-gradient elasticity for wave propagation in nanoporous graded double-nanobeam systems on elastic substrate. Compos. Struct. **168**, 885–892 (2017)
27. Zhu, X., Li, L.: Closed form solution for a nonlocal strain gradient rod in tension. Int. J. Eng. Sci. **119**, 16–28 (2017)
28. Li, X., Li, L., Hu, Y., Ding, Z., Deng, W.: Bending, buckling and vibration of axially functionally graded beams based on nonlocal strain gradient theory. Compos. Struct. **165**, 250–265 (2017)
29. Lu, L., Guo, X., Zhao, J.: A unified nonlocal strain gradient model for nanobeams and the importance of higher order terms. Int. J. Eng. Sci. **119**, 265–277 (2017)
30. Zhu, X., Li, L.: On longitudinal dynamics of nanorods. Int. J. Eng. Sci. **120**, 129–145 (2017)
31. Li, L., Hu, Y., Ling, L.: Flexural wave propagation in small-scaled functionally graded beams via a nonlocal strain gradient theory. Compos. Struct. **133**, 1079–1092 (2015)
32. Li, L., Hu, Y.: Buckling analysis of size-dependent nonlinear beams based on a nonlocal strain gradient theory. Int. J. Eng. Sci. **97**, 84–94 (2015)
33. Farajpour, A., Yazdi, M.H., Rastgoo, A., Mohammadi, M.: A higher-order nonlocal strain gradient plate model for buckling of orthotropic nanoplates in thermal environment. Acta Mech. **227**(7), 1849–1867 (2016)
34. Zaera, R., Fernández-Sáez, J., Loya, J.A.: Axisymmetric free vibration of closed thin spherical nano-shell. Compos. Struct. **104**, 154–161 (2013)
35. Ke, L.L., Wang, Y.S., Reddy, J.N.: Thermo-electro-mechanical vibration of size-dependent piezoelectric cylindrical nanoshells under various boundary conditions. Compos. Struct. **116**, 626–636 (2014)
36. Rouhi, H., Ansari, R., Darvizeh, M.: Analytical treatment of the nonlinear free vibration of cylindrical nanoshells based on a first-order shear deformable continuum model including surface influences. Acta Mech. **227**(6), 1767 (2016)
37. Rouhi, H., Ansari, R., Darvizeh, M.: Nonlinear free vibration analysis of cylindrical nanoshells based on the Ru model accounting for surface stress effect. Int. J. Mech. Sci. **113**, 1–9 (2016)
38. Mehralian, F., Beni, Y.T., Ansari, R.: Size dependent buckling analysis of functionally graded piezoelectric cylindrical nanoshell. Compos. Struct. **152**, 45–61 (2016)
39. Farajpour, A., Rastgoo, A., Mohammadi, M.: Vibration, buckling and smart control of microtubules using piezoelectric nanoshells under electric voltage in thermal environment. Phys. B Condens. Matter **509**, 100–114 (2017)
40. Sun, J., Lim, C.W., Zhou, Z., Xu, X., Sun, W.: Rigorous buckling analysis of size-dependent functionally graded cylindrical nanoshells. J. Appl. Phys. **119**(21), 214303 (2016)
41. Atmane, H.A., Tounsi, A., Bernard, F.: Effect of thickness stretching and porosity on mechanical response of a functionally graded beams resting on elastic foundations. Int. J. Mech. Mater. Des. **13**(1), 71–84 (2017)
42. Mechab, I., Mechab, B., Benaissa, S., Serier, B., Bouiadjra, B.B.: Free vibration analysis of FGM nanoplate with porosities resting on Winkler Pasternak elastic foundations based on two-variable refined plate theories. J. Braz. Soc. Mech. Sci. Eng. **38**(8), 2193–2211 (2016)
43. Barati, M.R.: On wave propagation in nanoporous materials. Int. J. Eng. Sci. **116**, 1–11 (2017)